Supplementary Information for "Variability in interseismic strain accumulation rate and style along the Altyn Tagh Fault"

Lin Shen[1*], Andrew Hooper[1], John Elliott[1], Tim Wright[1]

[1*]COMET, School of Earth and Environment, University of Leeds, Woodhouse Lane, Leeds, LS2 9JT, United Kingdom.

*Corresponding author(s). E-mail(s): L.Shen@leeds.ac.uk;

Contents

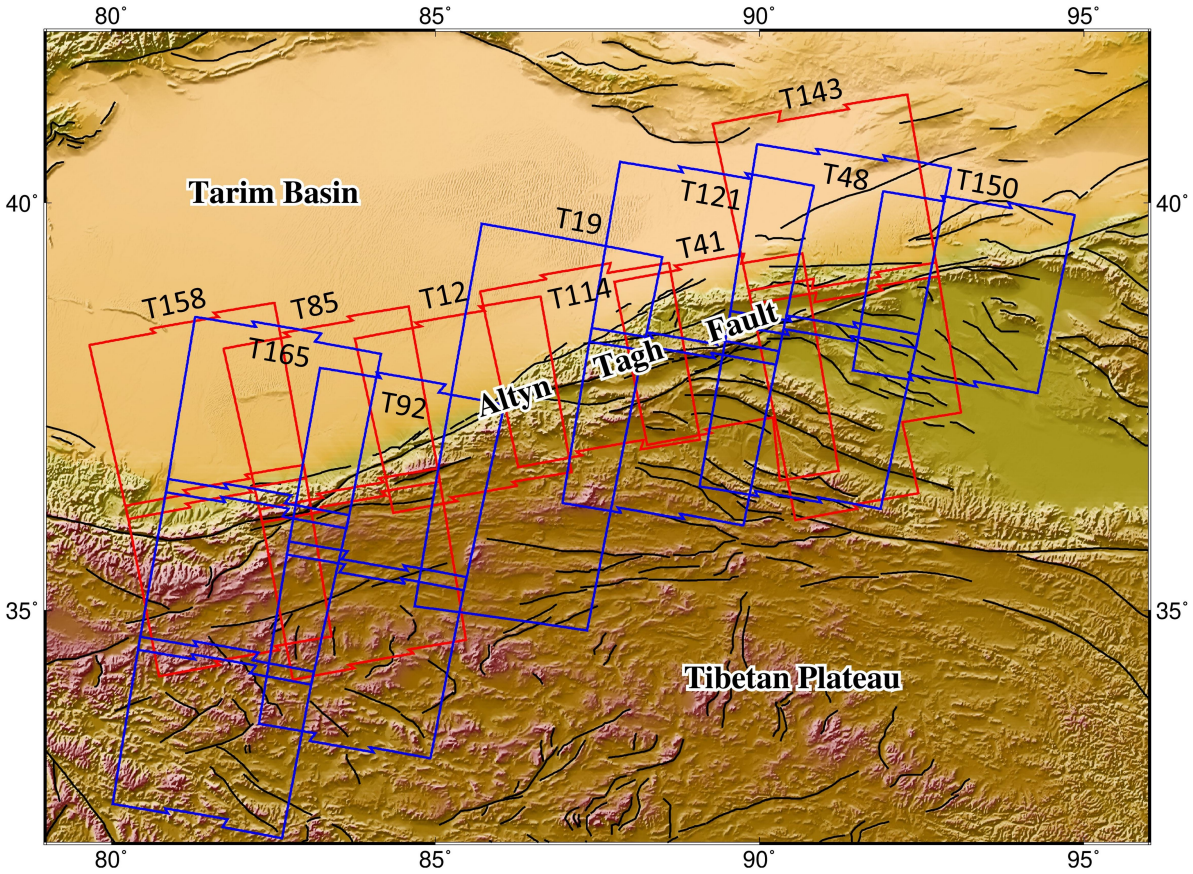

Supplementary Figure 1: Sentinel-1 data frames across the ATF, including 6 tracks in ascending (red polygons) and 6 tracks in descending (blue polygons).

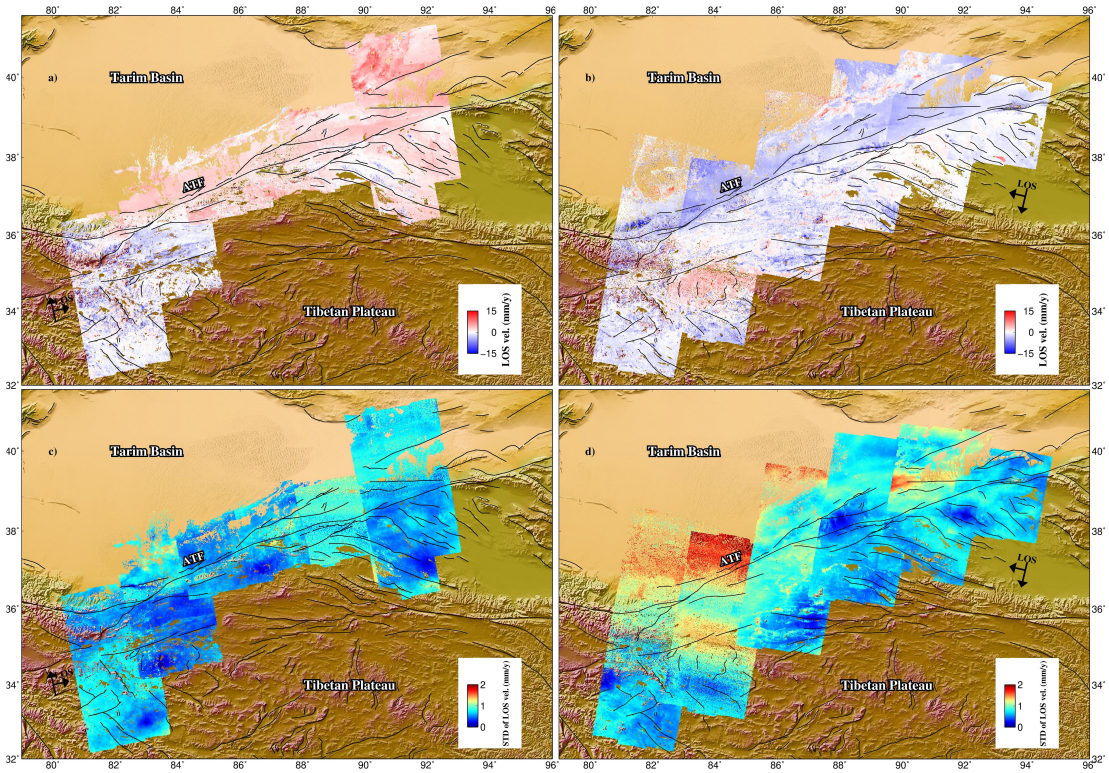

Supplementary Figure 2: Mosaicked InSAR LOS velocity fields in ascending (a) and descending (b) after removing the average offsets in overlapping areas. Positive values indicate the motion towards the satellite, whereas negative values show the motion away from the satellite. (c) and (d) are the estimated standard deviation of velocities accordingly using the percentile bootstrap method.

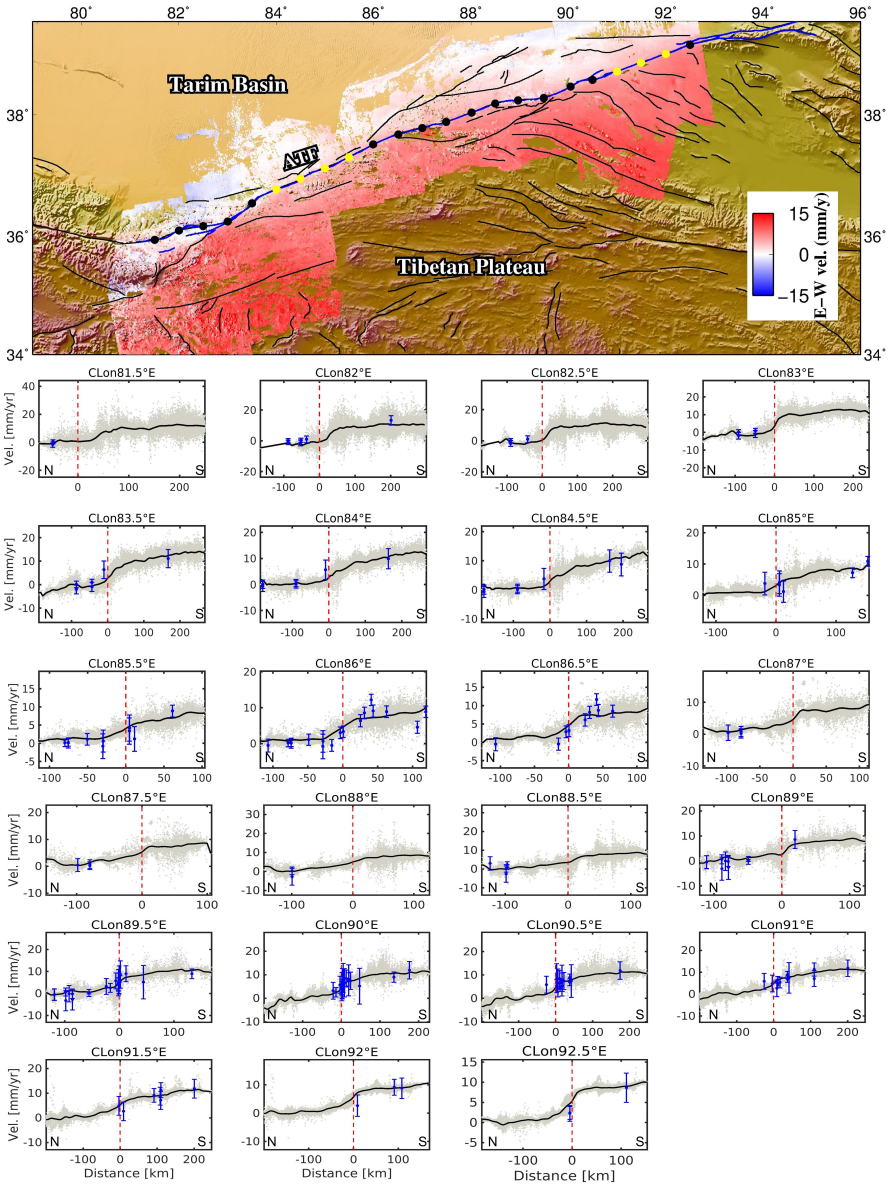

Supplementary Figure 3: Fault-parallel velocity profiles of the ATF derived from the east-west velocity field. The black and yellow points indicate the fault location of each profile on the high-resolution fault trace of the ATF (blue lines). The yellow points indicate locations for which the profiles show additional strain localisation south of the ATF. In the profile panels, the grey points are the mean fault-parallel velocities of points projected from within a 50 km perpendicular distance onto each profile; the black bold line represents the mean velocities binned by every 5 km along the profile; the red dashed lines show the mapped fault locations of main ATF; the blue points are the resolved fault-parallel GPS velocities projected onto the profile with $\pm 2\sigma$ errorbars.

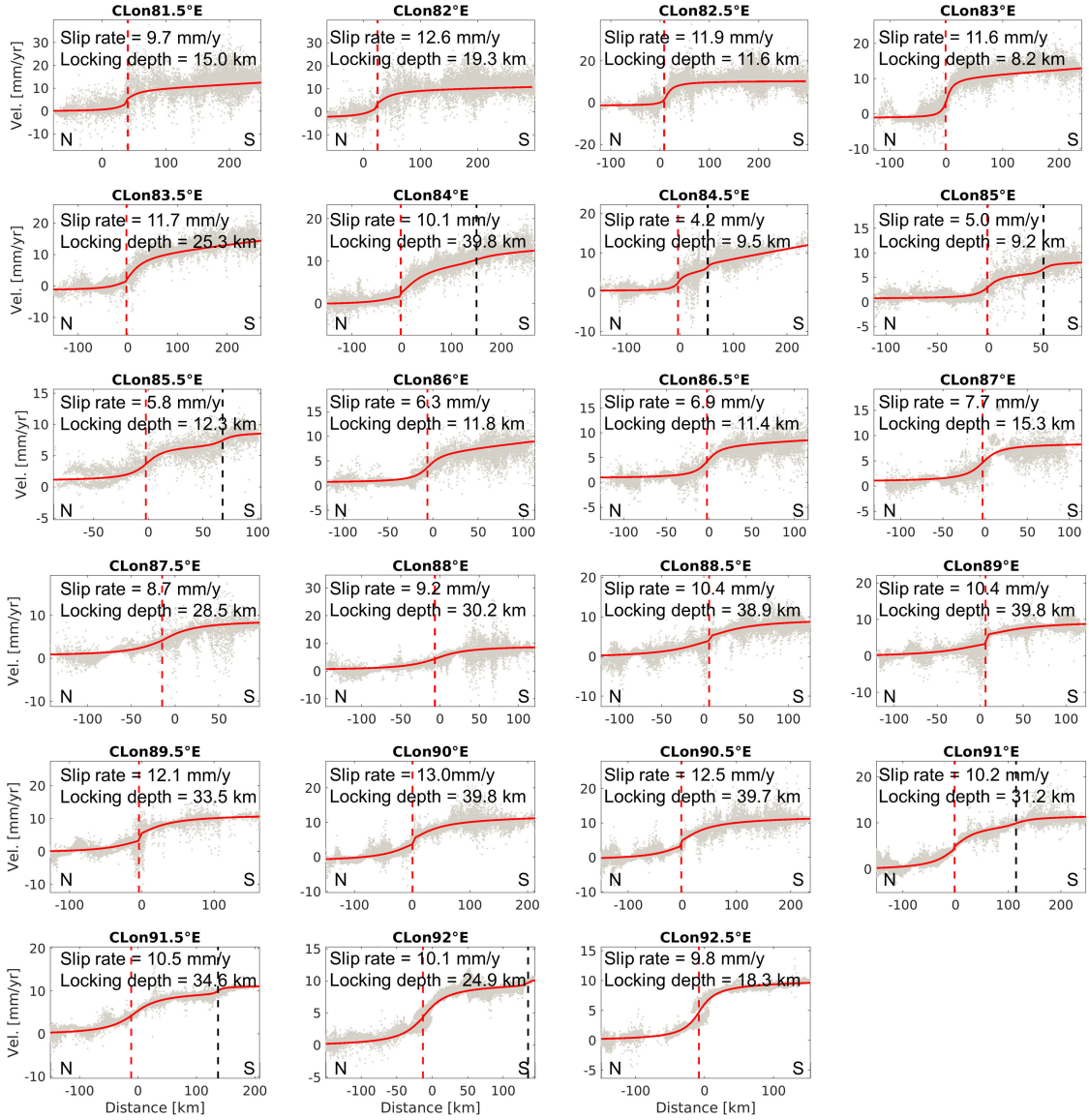

Supplementary Figure 4: The MAP solution for each fault-perpendicular profile (red curves). Red dashed lines represent the estimated locations of the buried dislocations along the ATF. Black dashed lines show the estimated locations of the buried dislocation of the additional strain on these profiles.

Supplementary Figure 5: Marginal probability distributions of each profile. Abbreviations of labels include 'S rate (Slip rate)', 'L depth (Locking depth)', 'H shifts (Horizontal shifts)', 'S offset (Static offset)', 'R ratio (Rigidity ratio)', 'C L depth (Creeping depth)', 'C rate (Creep rate)', 'R rate (Rotation rate)', 'A L depth (Additional locking depth)','A S rate (Additional slip rate)' and 'A H shifts (Additional horizontal shifts)'.

(a) At 81.5 °E.

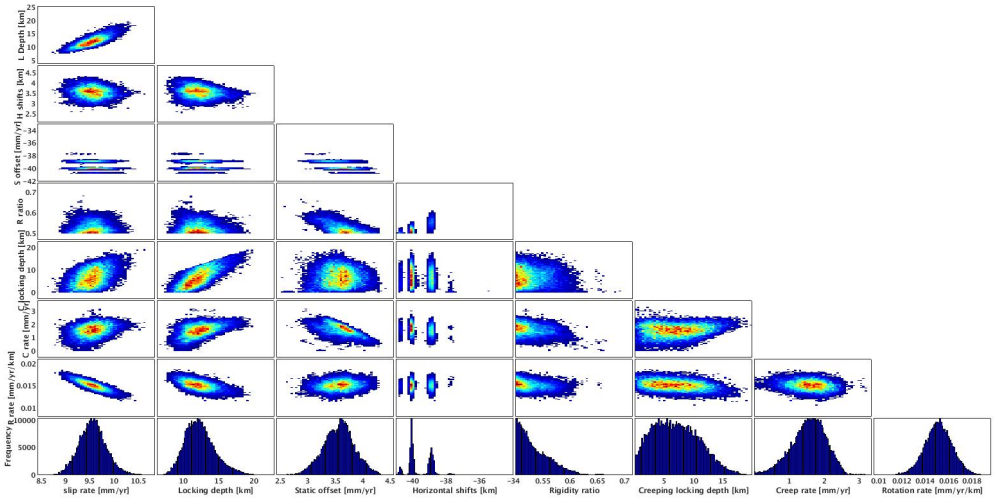

(b) At 82 °E.

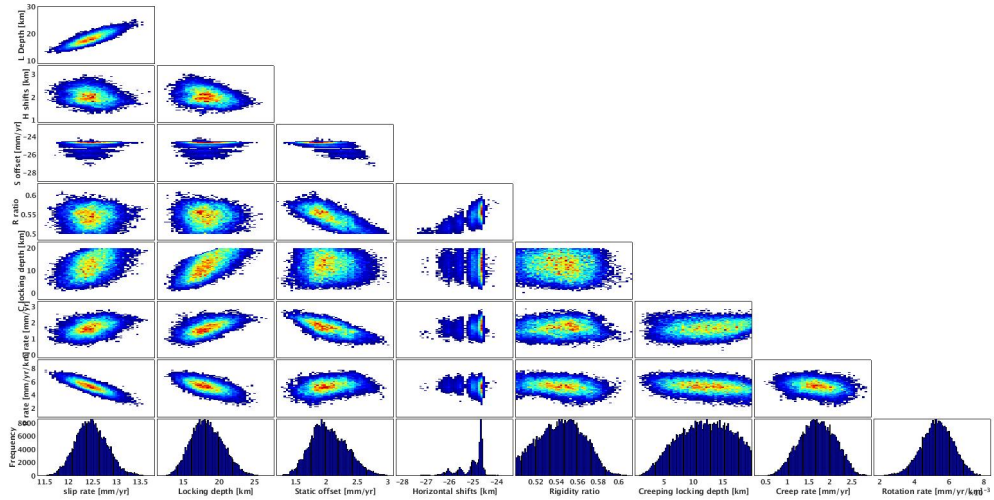

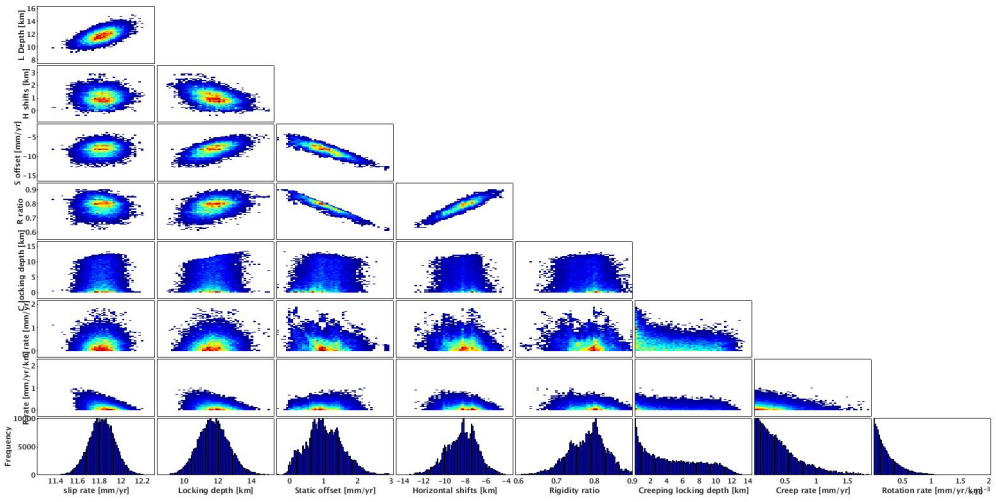

(c) At 82.5 °E.

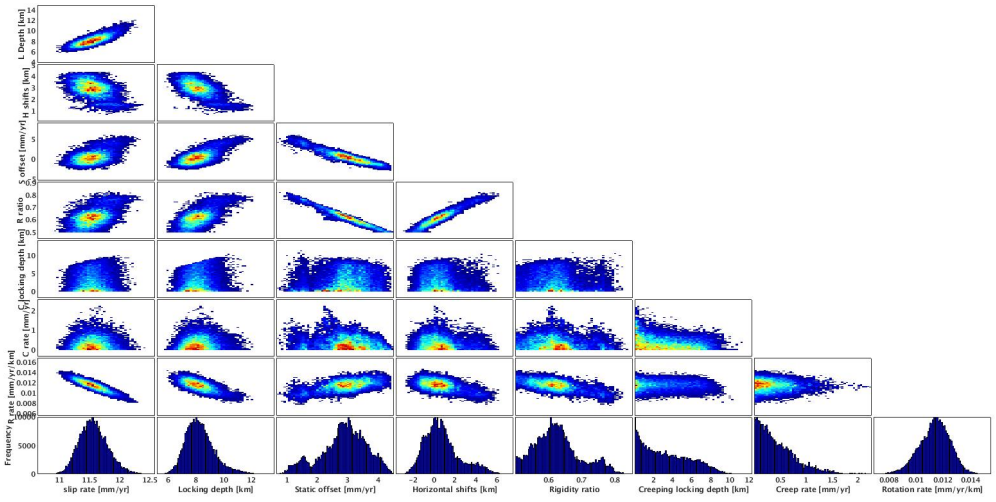

(d) At 83 °E.

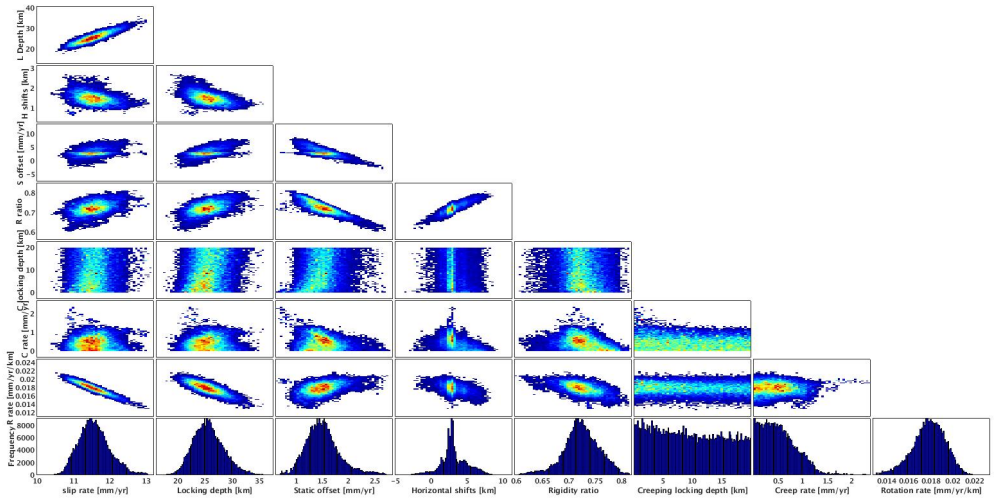

(e) At 83.5 °E.

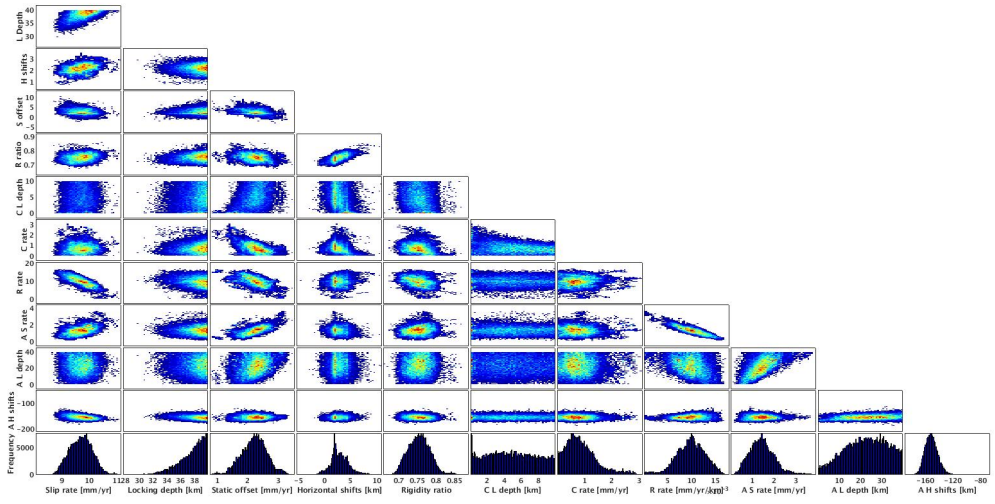

(f) At 84 °E.

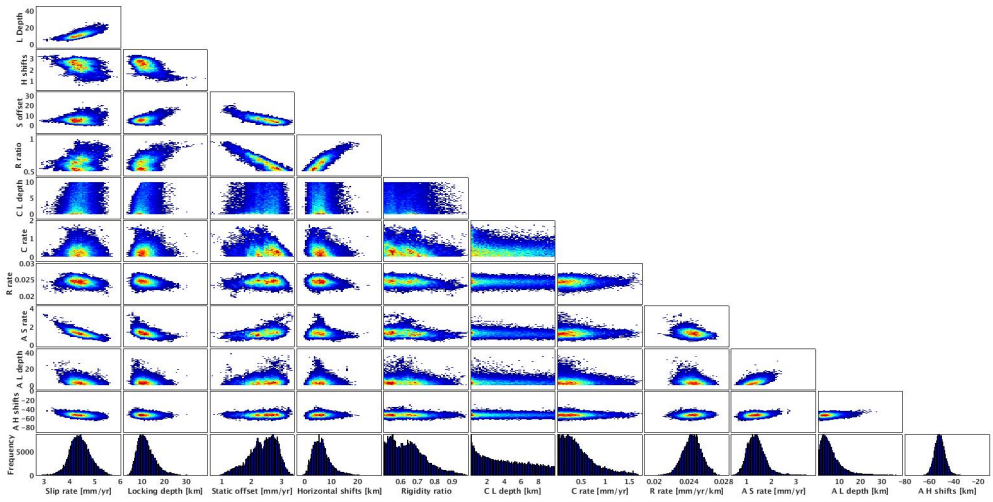

(g) At 84.5 °E.

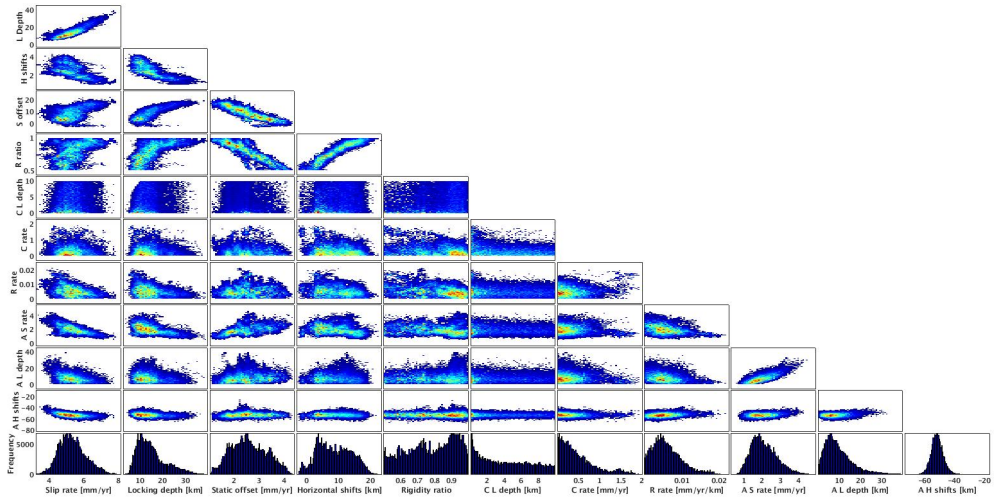

(h) At 85 °E.

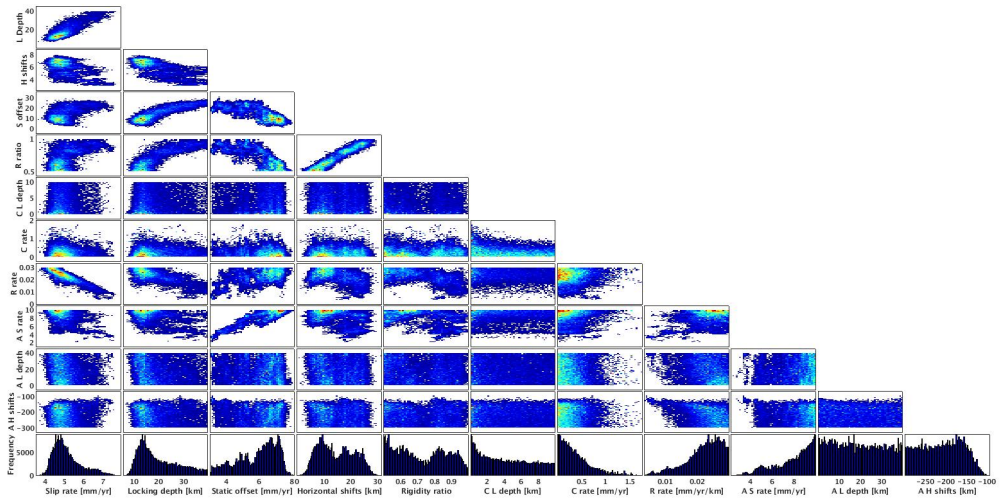

(i) At 85.5 °E.

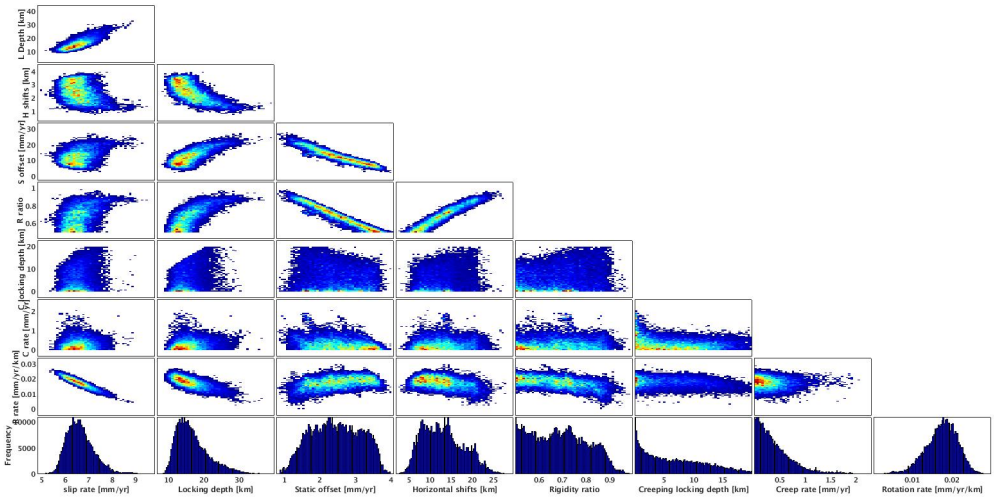

(j) At 86 °E.

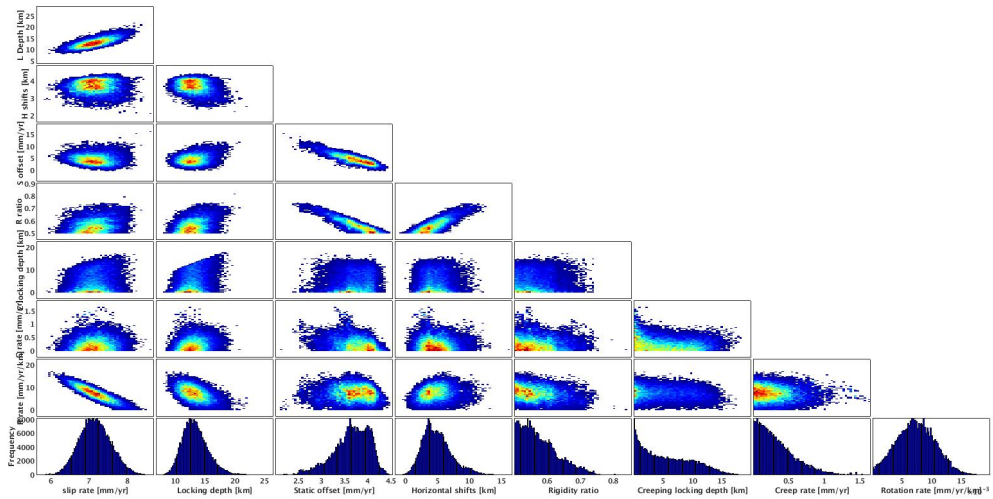

(k) At 86.5 °E.

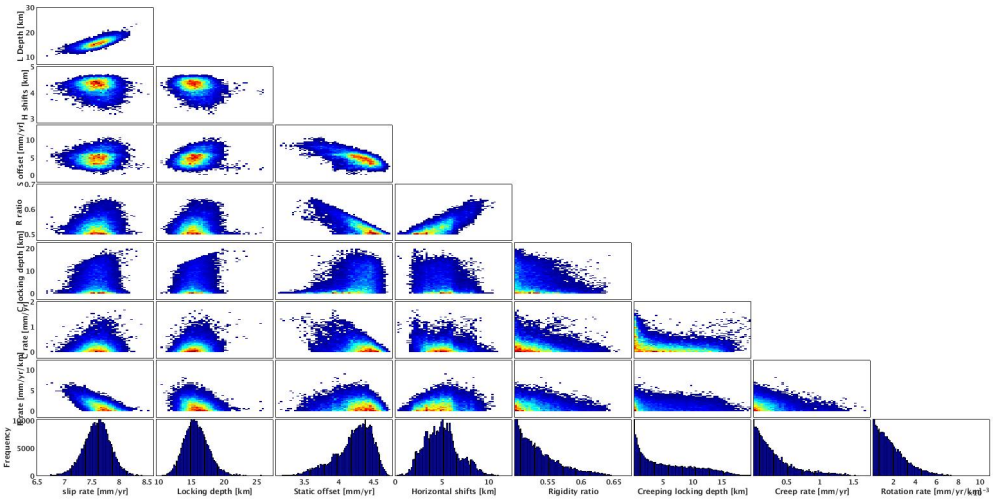

(l) At 87 °E.

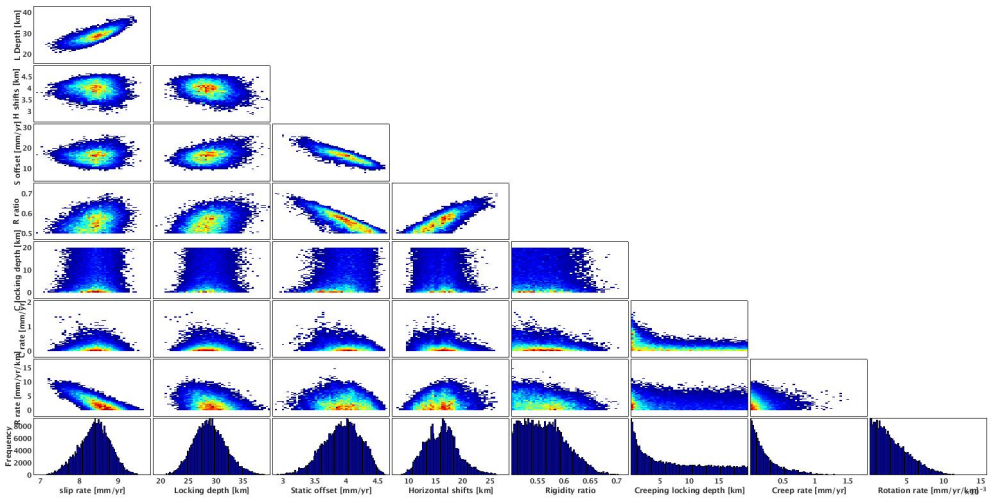

(m) At 87.5 °E.

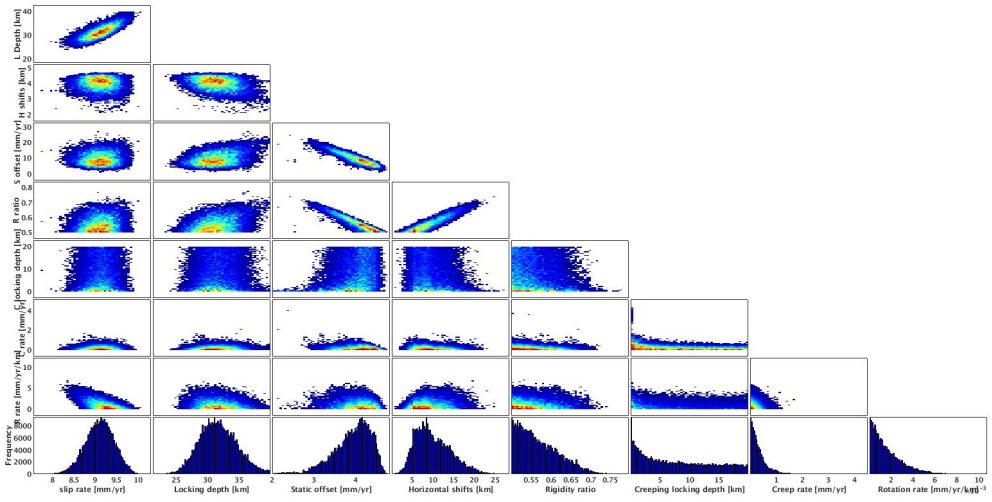

(n) At 88 °E.

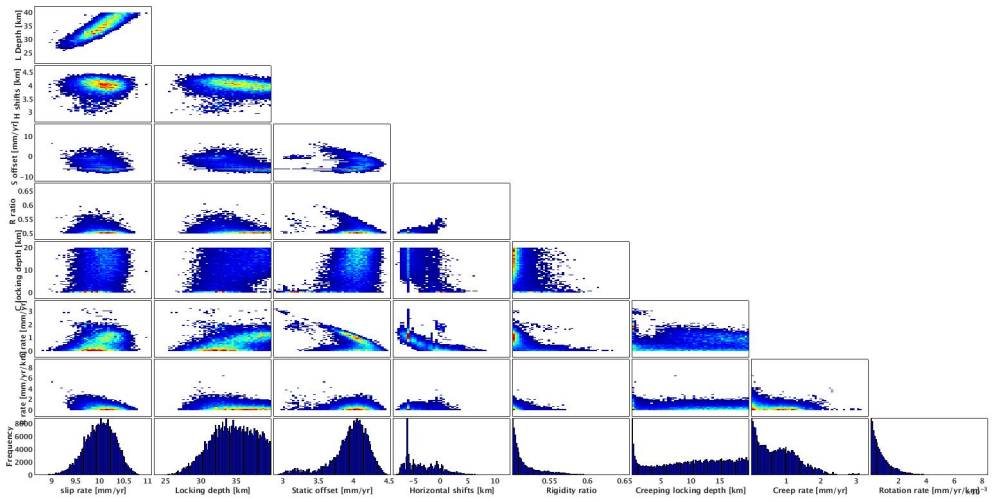

(o) At 88.5 °E.

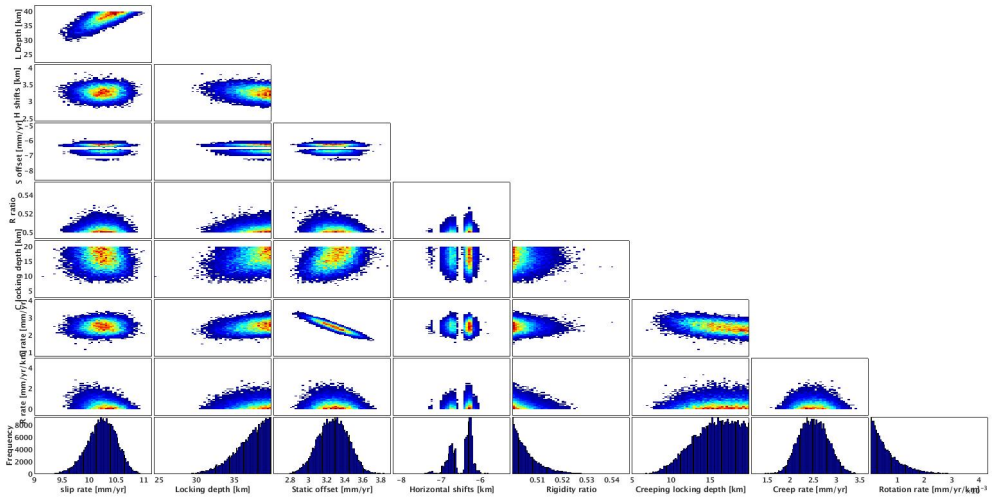

(p) At 89 °E.

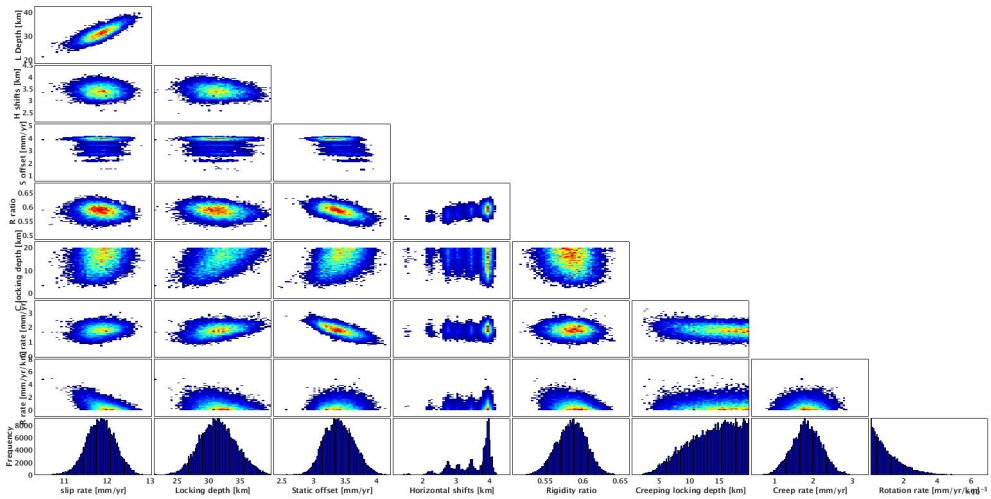

(q) At 89.5 °E.

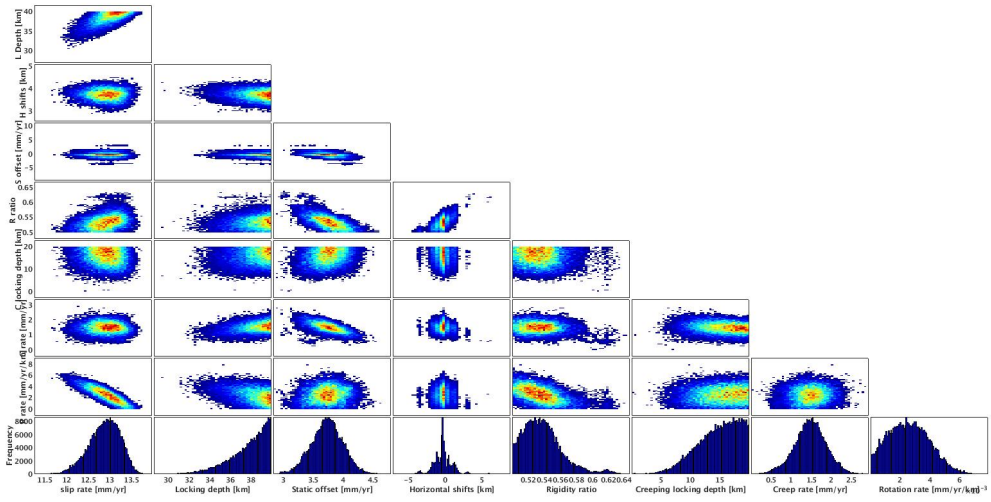

(r) At 90 °E.

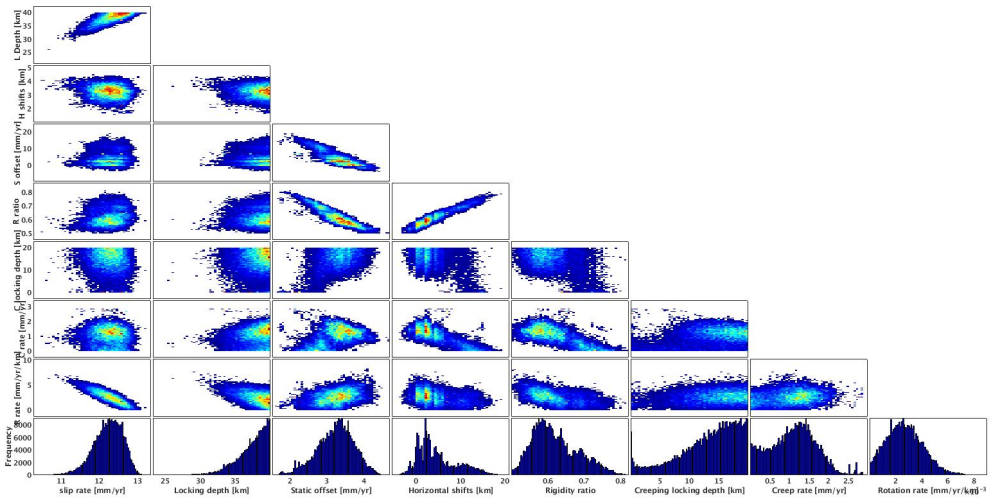

(s) At 90.5 °E.

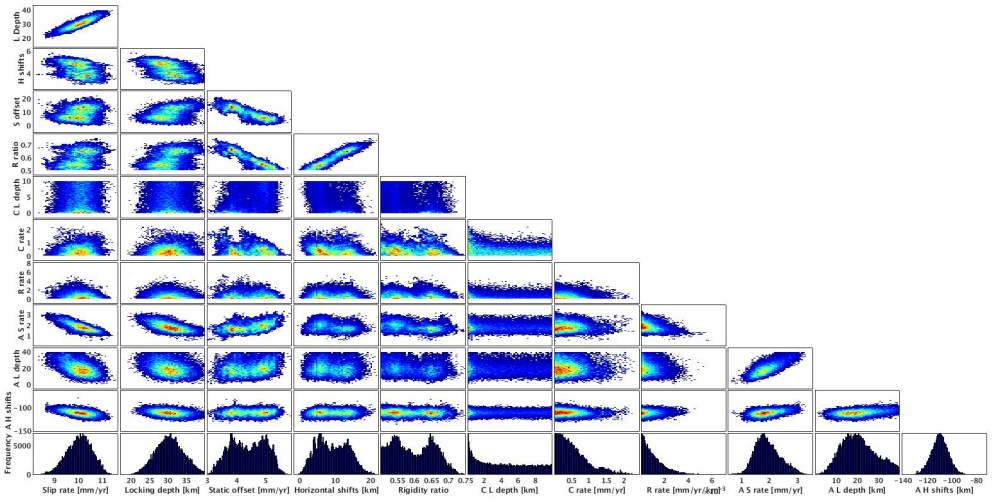

(t) At 91 °E.

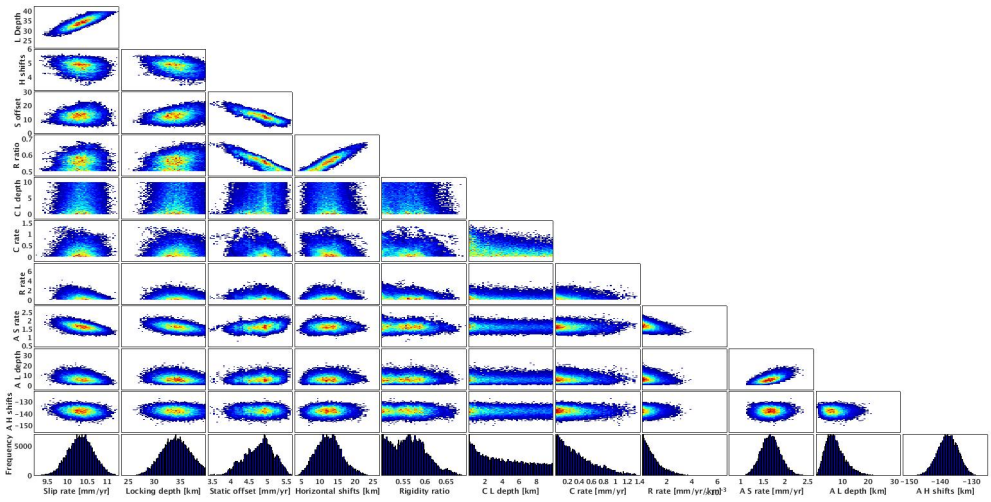

(u) At 91.5 °E.

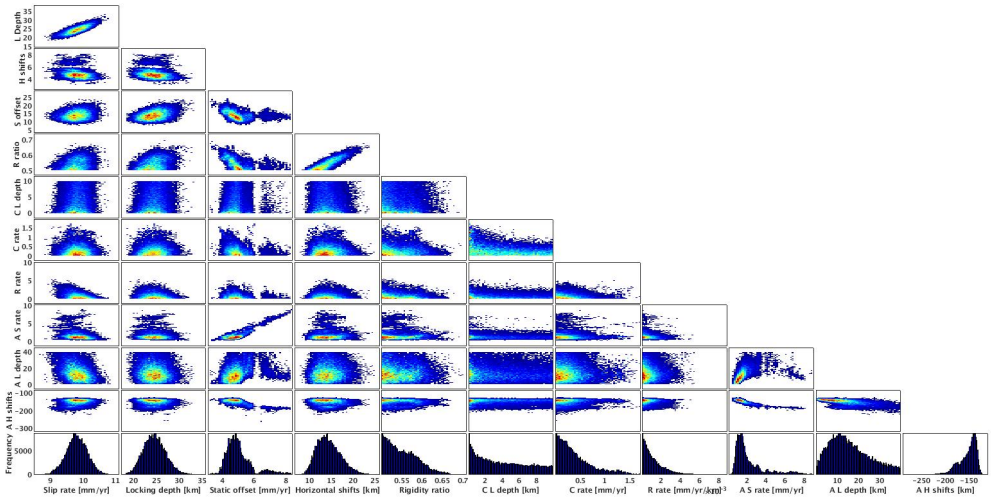

(v) At 92 °E.

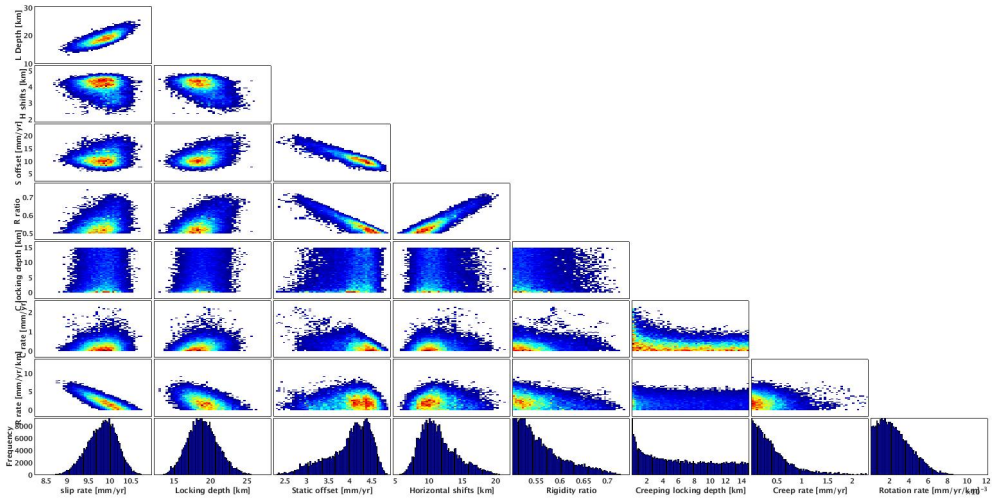
L Depth [km]
H shifts [km]
S offset [mm/yr]
R ratio
Locking depth [km]
Creep rate [mm/yr]
Rotation rate [mm/yr/kpl]
Frequency
slip rate [mm/yr]
Locking depth [km]
Static offset [mm/yr]
Horizontal shifts [km]
Rigidity ratio
Creeping locking depth [km]
Creep rate [mm/yr]
Rotation rate [mm/yr/kpl]$^{-3}$

(w) At 92.5 °E.

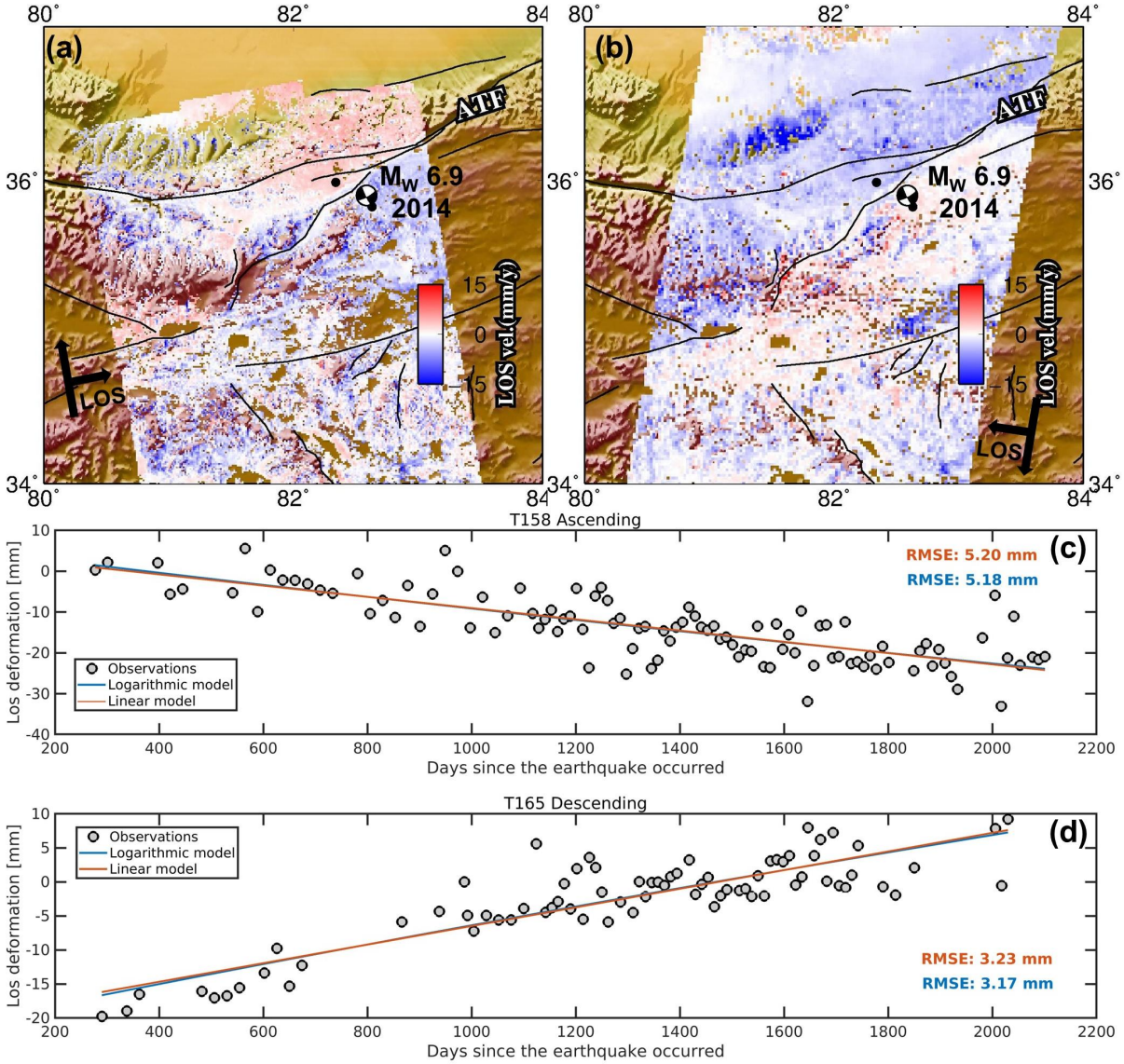

Supplementary Figure 6: Temporal evolution of LOS displacement between two sites on either side of the south-western segment of the ATF. (a) and (b) show the InSAR LOS velocity fields of the ascending track 158 and the descending track 165, respectively. Black points in (a) and (b) represent the locations of two sites. The focal mechanism indicates the 2014 M_w 6.9 Yutian earthquake. Black-gray scatters in (c) and (d) show the time series of the relative LOS displacement between the two sites for the ascending and descending track, respectively. Blue and orange lines represent the best fit logarithmic and linear model to the time series, respectively.

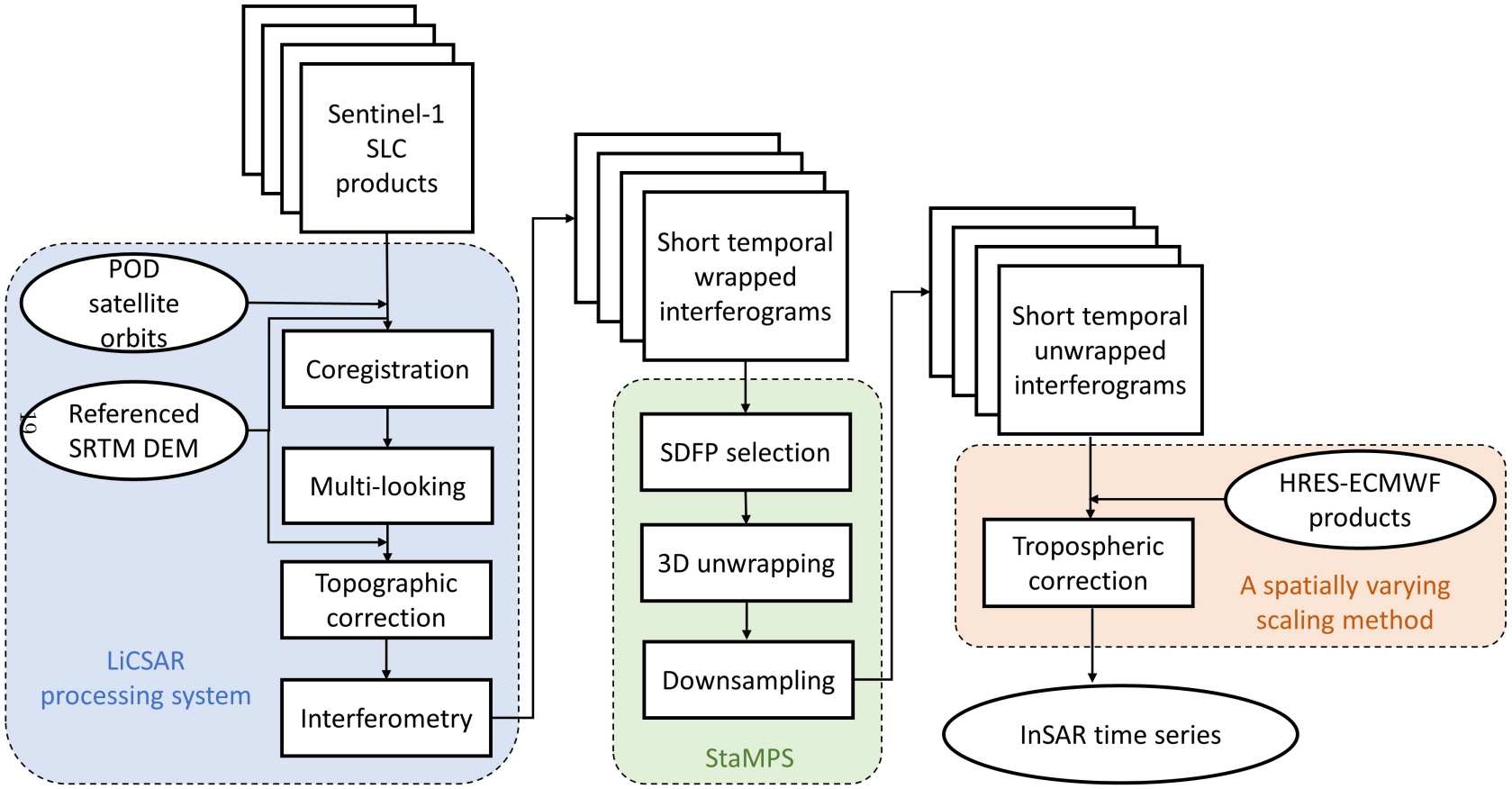

Supplementary Figure 7: A work flow diagram illustrating the main steps of InSAR processing from Sentinel-1 Simple Look Complex (SLC) products to time-series.

Supplementary Figure 8: Small baseline subset networks of the individual tracks. The red circles represent the epochs of SAR acquisitions and the black lines indicate the generated small temporal baseline interferograms.

(a)

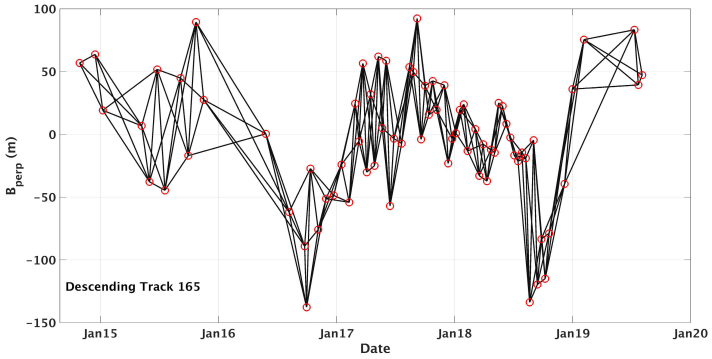

(b)

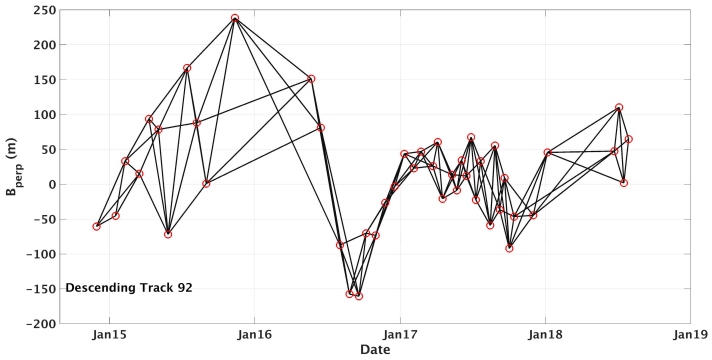

(c)

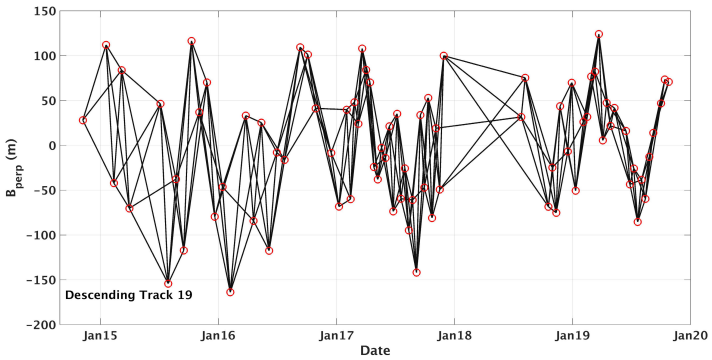

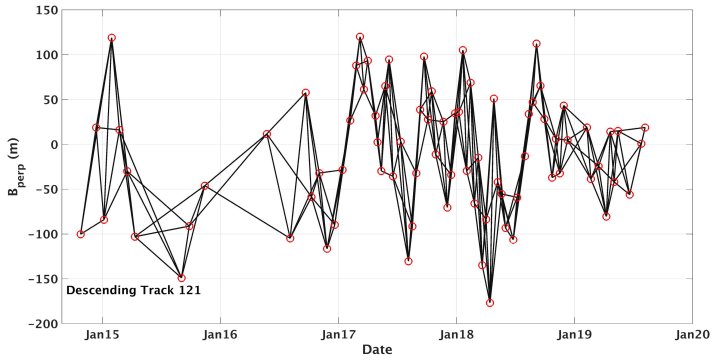
150
100
50
0
−50
−100
−150
−200
B perp (m)
Descending Track 121
Jan15
Jan16
Jan17
Jan18
Jan19
Jan20
Date

(d)

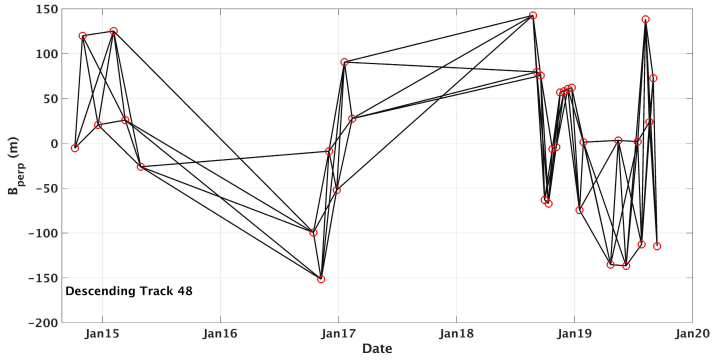
150
100
50
0
−50
−100
−150
−200
B perp (m)
Descending Track 48
Jan15
Jan16
Jan17
Jan18
Jan19
Jan20
Date

(e)

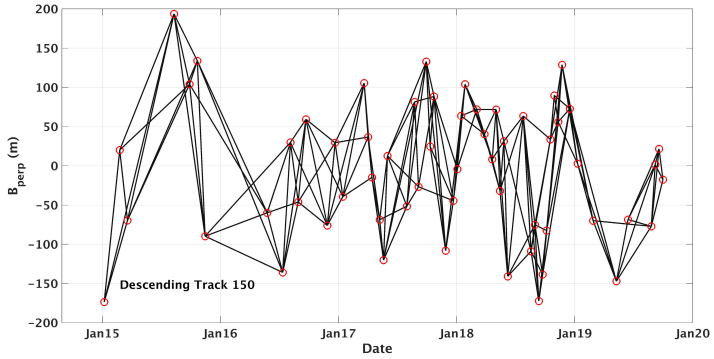
200
150
100
50
0
−50
−100
−150
−200
B perp (m)
Descending Track 150
Jan15
Jan16
Jan17
Jan18
Jan19
Jan20
Date

(f)

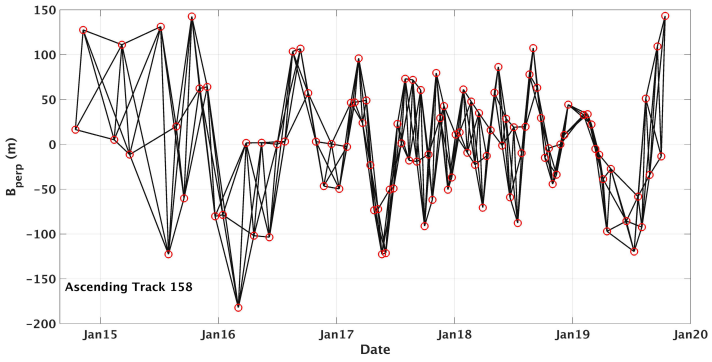
150
100
50
0
−50
−100
−150
−200
B perp (m)
Ascending Track 158
Jan15
Jan16
Jan17
Jan18
Jan19
Jan20
Date

(g)

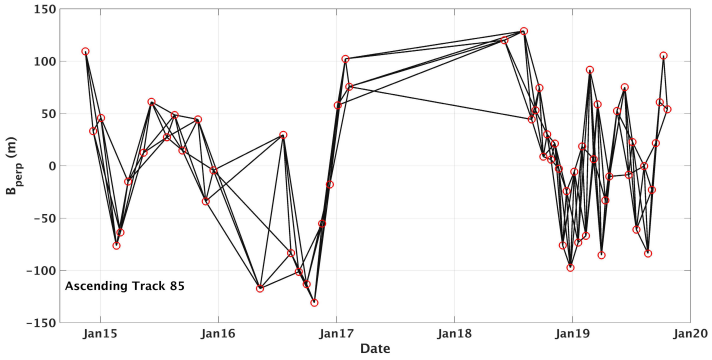
150
100
50
0
−50
−100
−150
B perp (m)
Ascending Track 85
Jan15
Jan16
Jan17
Jan18
Jan19
Jan20
Date

(h)

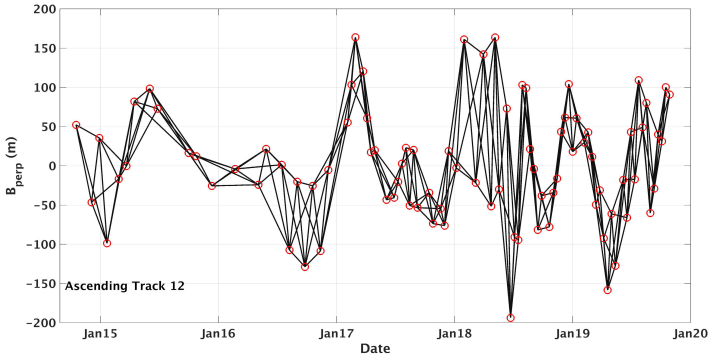
200
150
100
50
0
−50
−100
−150
−200
B perp (m)
Ascending Track 12
Jan15
Jan16
Jan17
Jan18
Jan19
Jan20
Date

(i)

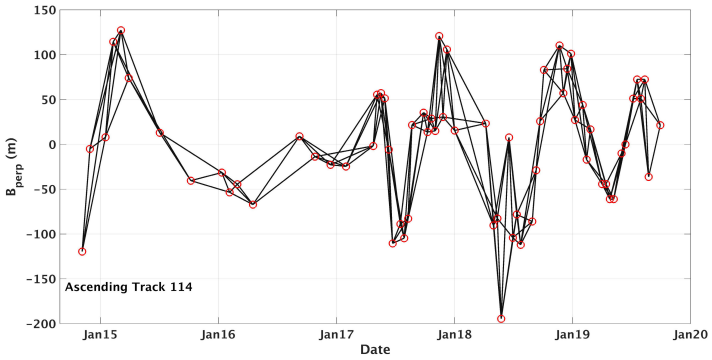
150
100
50
0
−50
−100
−150
−200
B perp (m)
Ascending Track 114
Jan15
Jan16
Jan17
Jan18
Jan19
Jan20
Date

(j)

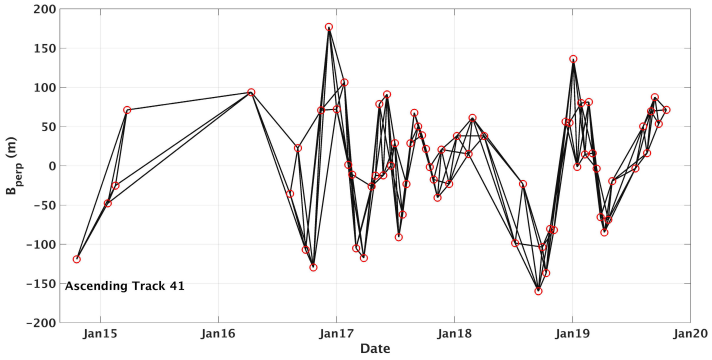
200
150
100
50
0
−50
−100
−150
−200
B perp (m)
Ascending Track 41
Jan15
Jan16
Jan17
Jan18
Jan19
Jan20
Date

(k)

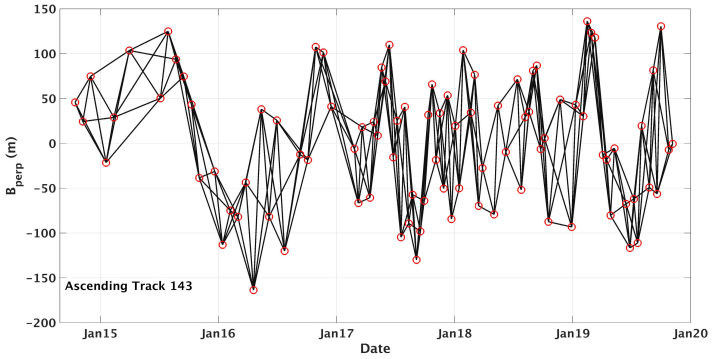
150
100
50
0
−50
−100
−150
−200
B perp (m)
Ascending Track 143
Jan15
Jan16
Jan17
Jan18
Jan19
Jan20
Date

(l)

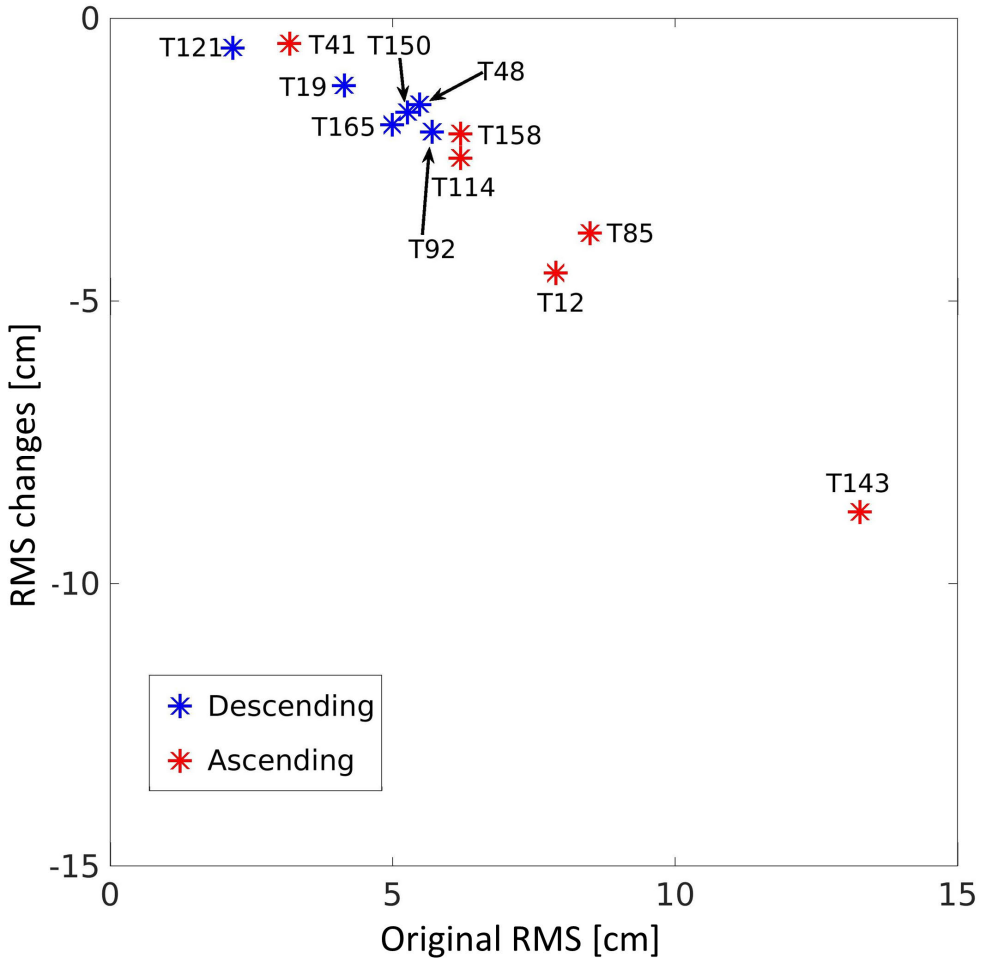

Supplementary Figure 9: RMS comparisons of interferograms for individual tracks before and after tropospheric corrections. All tracks show a reduction in the RMS after the correction is applied.

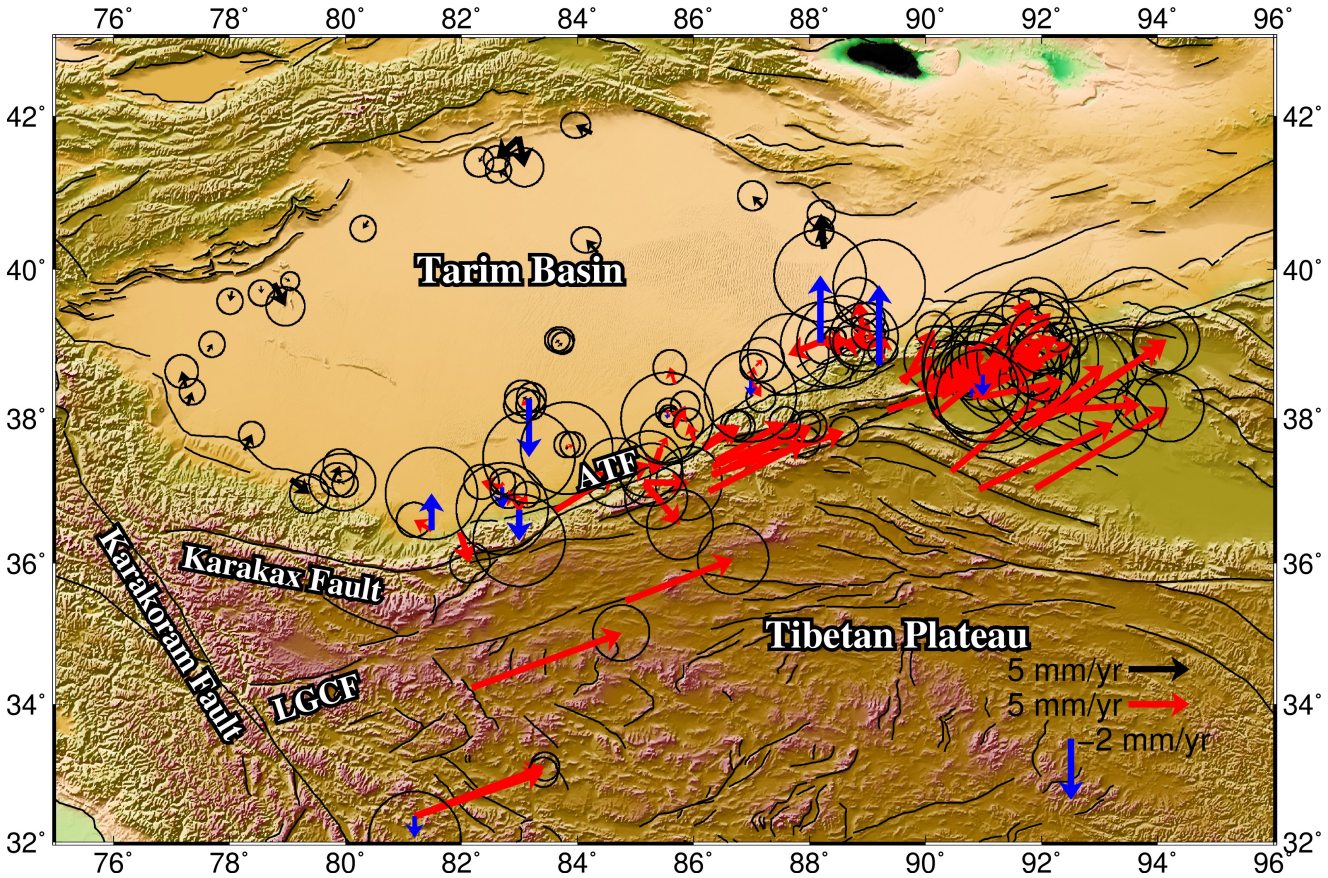

Supplementary Figure 10: GPS velocity map. Black vectors show horizontal velocities of the 28 GPS sites used to define the Tarim Basin reference frame. Red vectors and blue vectors represent horizontal velocities of the 84 available GPS sites and vertical velocities of the 23 available GPS observations used to determine the linear planes for each track, respectively. All velocities are plotted in the defined Tarim Basin reference frame at 68 % confidence level.

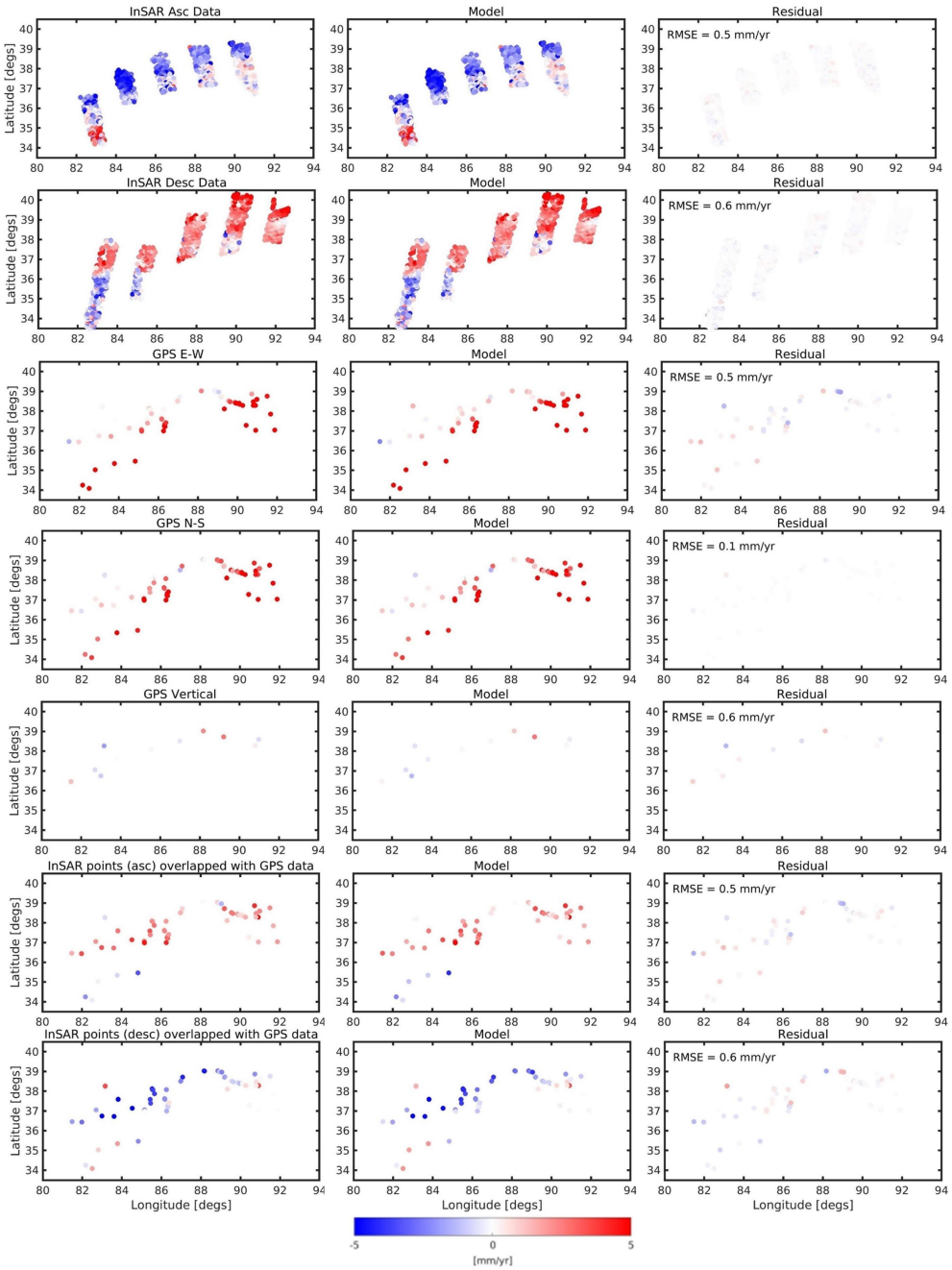

Supplementary Figure 11: The fit of the model to the data points in the inversion for long wavelength trends. Panels in the first and the second rows show the fit of the model to the InSAR points selected from the overlapping region between adjacent tracks; Panels in the third to the fifth rows indicate the fit of the model to the GPS data; Panels in the last two rows show the fit of the model to the InSAR points covered by the GPS sites in ascending and descending, respectively.

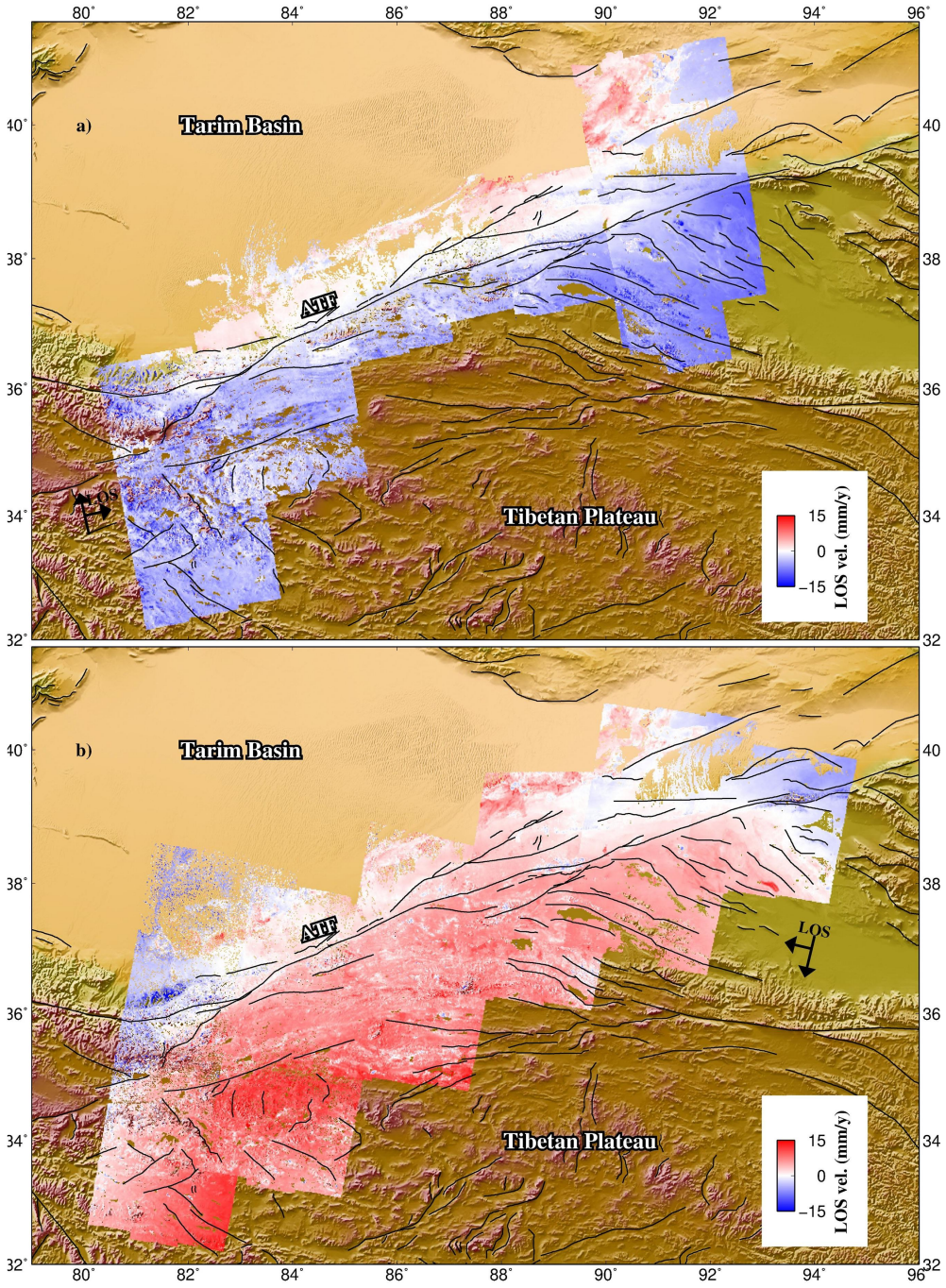

Supplementary Figure 12: Mosaicked InSAR LOS velocity fields of ascending (a) and descending (b) in the Tarim reference after removing the inverted linear planes from each track. Positive values indicate motion towards the satellite.

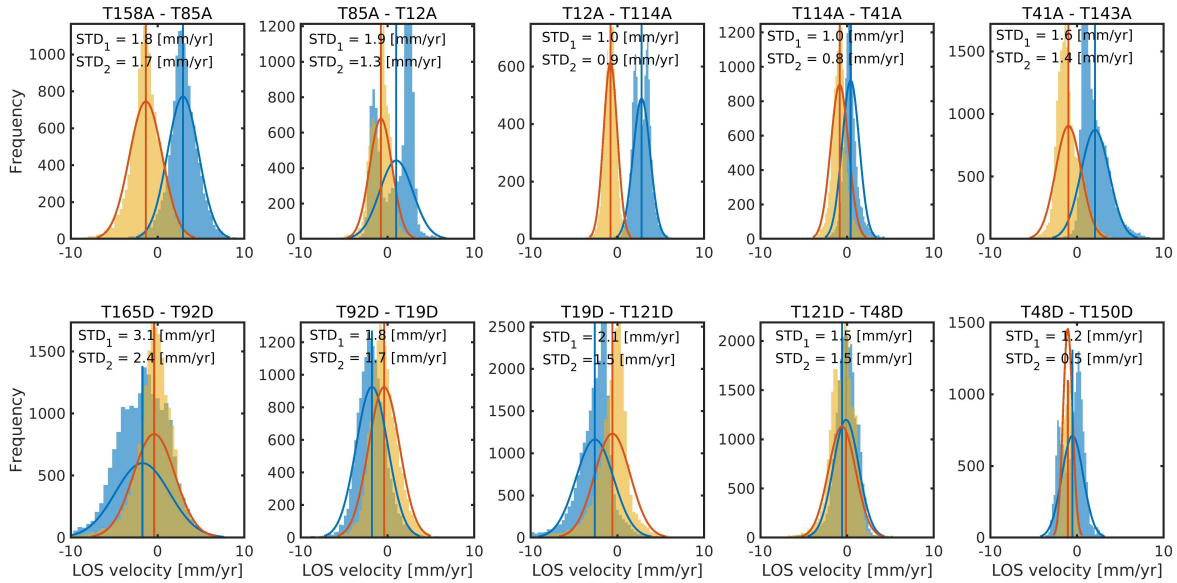

Supplementary Figure 13: Comparison of the LOS velocity differences in the overlapping region between adjacent tracks before and after velocity mosaicking. Blue histograms show the original differences along with the Gaussian distribution fit (blue curves), whereas the yellow-orange colour features the differences after removing inverted linear planes. The blue and orange lines indicate the mean value of the corresponding Gaussian distribution. STD_1 and STD_2 show the standard deviation of each estimated Gaussian distribution before and after velocity mosaicking, respectively. The mean of each is expected to be non-zero due to the different incidence angles.